Anisotropic Curvature Motion for Structure Enhancing Smoothing of 3D MR Angiography Data

Oliver Nemitz, Martin Rumpf*, Tolga Tasdizen, and Ross Whitaker**

University of Bonn, University of Utah

Abstract. We propose a novel concept of shape prior for the processing of tubular structures in 3D images. It is based on the notion of an anisotropic area energy and the corresponding geometric gradient flow. The anisotropic area functional incorporates a locally adapted template as a shape prior for tubular vessel structures consisting of elongated, ellipsoidal shape models. The gradient flow for this functional leads to an anisotropic curvature motion model, where the evolution is driven locally in direction of the considered template. The problem is formulated in a level set framework, and a stable and robust method for the identification of the local prior is presented. The resulting algorithm is able to smooth the vessels, pushing solution toward elongated cylinders with round cross sections, while bridging gaps in the underlying raw data. The implementation includes a finite-element scheme for numerical accuracy and a narrow band strategy for computational efficiency.

1 Introduction

Segmentation of blood vessels from medical images, such as magnetic resonance angiography (MRA) and computed tomography (CT) is a challenging problem with several applications that are very important in diagnosis and surgery. Detection of stenosis and aneurysm, and measuring tortuosity are examples where an accurate segmentation of the vasculature can help in the diagnosis and quantification of certain disease-related characteristics of vessel geometry, such as diameter [25] Also, in surgical applications, it is important to have accurate estimates of the locations of vessels.

Many different approaches have been proposed for segmenting vessels, or more generally tube-like structures, in the literature. We give a brief overview in Section 1.1. In this paper, we propose the use of a new prior model for tubular geometry that can be used to post process segmented volumes or as a component of an active contour models. Active contour models typically start with an initial model and propagate the model according to some partial differential equation (PDE). This PDE is typically constructed as a weighted sum of two terms: (i) a data term that drives the model towards the boundaries of the shape to be segmented, and (ii) a shape prior (or model) that ensures the smoothness of the resulting surface. The latter is critical due to noise and incomplete data, and the effectiveness of such priors can be evaluated independently of the data term by studying the incremental effects of their application to noisy input data.

* Mail: {oliver.nemitz,martin.rumpf}@ins.uni-bonn.de
** Mail: tolga@sci.utah.edu,whitaker@cs.utah.edu

Thus, this paper focuses on introducing a novel shape prior for level set surfaces that is specifically designed to represent tubular structures and studies the effectiveness of this model as a surface smoothing process. The proposed method is derived as the gradient flow for a suitable geometric penalty function that includes a local, scale invariant classification of the geometry using the approach of Wulff shapes, known from material science. It incorporates the corresponding Frank diagram directly in the geometric energy density. The paper presents the mathematics of this approach, the associated numerical scheme, and results on synthetic and real data.

1.1 Related Work

Many different approaches for filtering and segmenting vascular structures from medical images have been proposed in the literature, and here we give a brief overview of the trends. One approach to vascular segmentation is to track the centerlines of vessels with oriented filters [4]. Alternatively, morphological image processing has been proposed for salient path finding [11]. Second-order differential structure of image intensity has been used in the form of curvature maxima [20] and multiscale Hessians [21, 17]. As in a variety of image segmentation problems, vascular segmentation has been approached using active contours [14, 18] and statistics [5]. Several authors have introduced filtering methods for denoising and enhancing curvilinear structures in images [12, 21, 15]. Generally, denoising methods are used as a pre-processing step for segmentation [15] or for visualization [21]. However, denoising or smoothing methods that are derived from a variational formulation can also be combined with a fitting term to perform segmentation based on deformable models [13]. The focus of this work is on geometric flows implemented with level-set surfaces, and a particularly relevant body of work is the work on surface deformation that uses level sets and incorporates various kinds of directional smoothing. Several authors have noted that mean curvature flow is not a suitable prior for thin, tubular structures, because it favors the principle curvature of greater magnitude and therefore tends to collape these vessels and break them into pieces early on in the processing. Whitaker [23], shows that a surface motion proportional to the normalized product of Gaussian and mean curvatures favors tubular structures. Other researchers have studied alternate formulations of anisotropic smoothing of level-set surfaces based on principle curvatures. For instance, Preusser and Rumpf [6] propose an anisotropic conductance tensor for this purpose and demonstrate the ability to preserve features, while Krissian *et al.*[16] propose a weighted combination of curvatures along each of the principle (and normal) directions. Ambrosio *et al.* [2] prove that a surface moving with a velocity equal to the minimum (magnitude) principle curvature minimizes the length of the center curve associated with very thin (in the limit) tubular structures. Lorigo *et al.* [18] use this idea for segmenting vascularature. They show that segmentation results, with level-set surface models, can be significantly improved by propagating the surface according to the minimum principal curvature, rather than the mean curvature. Their method includes a data term to reconnect vessels that appear broken in the initialization. This is necessary because the minimal curvature prior itself cannot force vessels to grow and reconnect. The same is true of all methods that are based on convex combinations of principle curvatures. One of the advantages of the proposed method is the ability to grow and reconnect gaps in tubular structures with

or without a data term. Of course, the inclusion of the data term would improve the resulting segmentations, but the data attachment is not the focus of this work, and in this paper we study only the effects of the various priors, which we use as a smoothing term.

More generally, this paper describes a framework in which local models of image structure give rise to variational expressions that can be used to force surfaces to adhere more closely to those models. In this way the framework could be extended to include various kinds of shape models and mechanisms for making decisions about appropriate models. Thus, the framework could be adapted to a variety of problems in which usual curvature-based flows are insufficient.

2 Methods

Given the raw data intensity function $I : \Omega \mapsto \mathbb{R}$ with $\Omega \subset \mathbb{R}^3$, we ask for a vessel description in terms of an iso-surface of a level set function $\phi : \Omega \mapsto \mathbb{R}$. As an initial guess we consider a threshold volume $\mathcal{V} = \{x \in \Omega : I(x) \geq \alpha\}$ and define ϕ as the signed distance function for the vessel boundary $\partial\mathcal{V}$. In general, simple thresholding will not always be a reliable way of finding initial segmentations. Nevertheless for the application case study provided here, we confine to this method for the initialization. Hence, the vessel set $\mathcal{V}$ is implicitly defined as sub volumes $\{x \in \Omega : \phi(x) \leq 0\}$. Unlike parameterized surfaces, surfaces defined with level set can change topology in a natural way. This is an important advantage in processing thin tubular surfaces with many topological artifacts such as breaks and extraneous pieces in the raw data. The method, we propose here, is based on several building blocks:

- the local classification of vessel radii and vessel directions,
- the definition of a local prior based on this classification,
- a gradient flow for the relaxation of this energy, including
- a localized volume preservation.

These building blocks are explained next.

2.1 Local classification of vessel radii and vessel directions

We aim to represent tubular vessel structures in MRA by elongated ellipsoid shapes as local priors. Thus, we have to identify the local orientation of the vessels to define correspondingly elongated ellipsoids. This classification is based on a moment analysis and underlying robust estimate of vessel radii.

Moment analysis. Given the image function I and a threshold α, that can be used to approximately separate the vessels from the background, we consider the characteristic function $\chi_{\mathcal{V}}$ for the vessel structures $\mathcal{V}$. From this characteristic function, we calculate the local first moment for each point x_0 as

$$M_{\mathcal{V}}(x_0) := \frac{1}{m_{\mathcal{V}}(x_0)} \int\limits_{B_r(x_0)} \chi_{\mathcal{V}}(x)(x - C_{\mathcal{V}}(x_0)) \otimes (x - C_{\mathcal{V}}(x_0))\, dx, \tag{1}$$

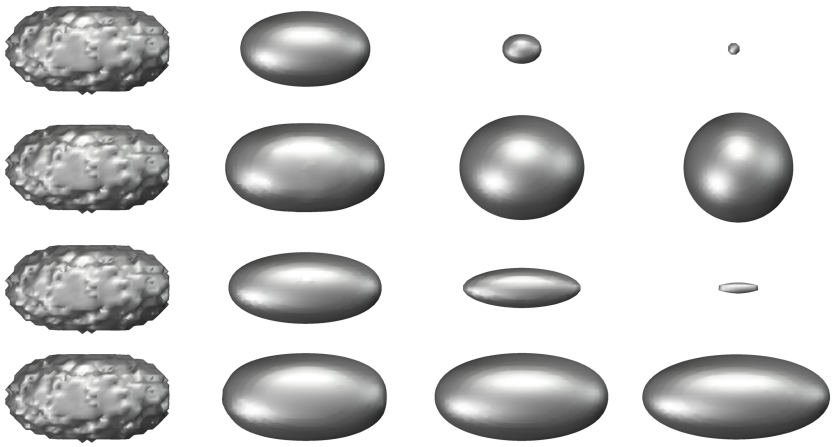

Fig. 1. Comparison of Mean Curvature Flows: The first row depicts the classical isotropic MCF, the second row the isotropic but volume-preserving MCF, whereas in the third and fourth row the anisotropic and volume-preserving anisotropic MCF can be seen.

where $m_{\mathcal{V}}(x) = \int_{B_r(x_o)} \chi_{\mathcal{V}}(x)\, dx$ is the mass and $C_{\mathcal{V}}(x_0)$ is the center of gravity of the distribution $\chi_{\mathcal{V}}$ in the ball $B_r(x_0)$. The eigenvectors $v_i, i = 1, 2, 3$ and eigenvalues $\lambda_1 \geq \lambda_2 \geq \lambda_3$ of this matrix, provide information about the shape and orientation of the mass distribution of $\chi_{\mathcal{V}}$ and thus of the vessel structures. If the mass is distributed uniformly, all eigenvalues will be approximately equal. If it is distributed as a disc, we have $\lambda_1 \approx \lambda_2 >> \lambda_3 \approx 0$. For details we refer to [7]. In case of a long cylindrical distribution, we get $\lambda_1 >> \lambda_2, \lambda_3 \approx 0$. Hence, for recognizing vessel structures which are supposed to be long cylindrical structures, we look at the ratio $c = \frac{\lambda_2+\lambda_3}{\lambda_1+\lambda_2+\lambda_3}$, which is close to 0 for long tubes. Consequently, for each point, if the ratio c is smaller than a threshold ε, we choose the eigenvector belonging to the biggest eigenvalue as direction of the vessels in x_0. Let us denote this directional field by v. If $c > \varepsilon$, we decide that there is no vessel at this point. In that case, we switch to ball shaped Wulff shapes and the corresponding isotropic mean curvature as the local driving force in the evolution. In a final step we normalize this vector field. Let us emphasize that we incorporate anisotropic smoothing, if and only if the directional field v gives a clear indication for an elongated tubular structure.

Vessel radius approximation. In the above analysis, the choice for the radius of the ball around a point x_0 in equation (1) is important. If this ball is too small, linear structures won't be recognized, whereas if the ball is too large, nearby but separate vessels will have an influence in the direction computation. Furthermore, it is not possible to choose a fixed radius for every pixel of the picture, because of varying vessel thicknesses. To estimate the local radius of vessels the above defined local mass of the characteristic function can be used. For a straight, infinitely long cylinder located at x_o of radius $R_v << R$, the expected mass of the characteristic function contained in $B_R(x_o)$

is approximately $2R\pi R_v^2$. Therefore, the vessel radius at x_o can be estimated as

$$R_{\mathcal{V}}(x_o, R) = \sqrt{\frac{m(x_o)}{2\pi R}}.$$

In practice, to improve robustness, we propose to evaluate $R_v(x_o, R)$ for a set of ball radii and choose the resulting median as vessel radius $R_{\mathcal{V}}$. For a single, noisy vessel we expect a small variance. However, if there are two vessels close by, R_v will be overestimated. Alternatively, if the vessel is broken up into smaller pieces then the above defined mass will be smaller than the true mass. As a result, the vessel radius will be underestimated (cf. Fig. 11 for a color coding of the radii estimate on MRA data). Nevertheless, we observe that the computation of the directional field v is not effected by this and remains numerically stable.

Smoothing the field of vessel directions. The image of vessel orientations is not smooth due to the noise in the data. Therefore, we consider a smoothing of the vessel directions. Here, we apply a Gaussian filter to the directions represented by the rank one matrices vv^T, where v is the dominant principal component of the structure tensor defined above. By doing so the filtered matrix field is generically of full rank. Thus, we again choose the eigenvector corresponding to the dominant eigenvalue as our final smoothed vector in x_0, (cf. Fig. 2 for the resulting directional field in case of a simple torus like tubular structure as a test data set).

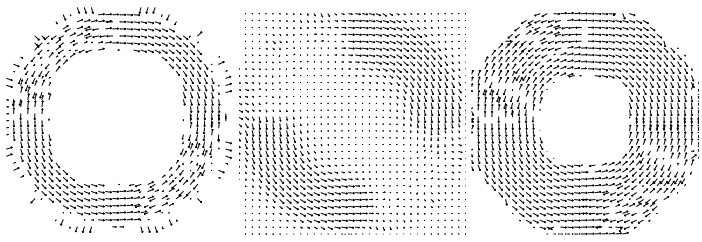

Fig. 2. Vectorfield on a cross section of a torus, left: original, middle: smoothed with Gaussian filter, right: smoothed with the described method

2.2 Defining a local prior

As mentioned above, we aim to represent blood vessel's structure locally by elongated ellipsoids. As the implicit representation of an ellipsoid with half-axis $a, b, c \in \mathbb{R}$, we choose a function γ as follows:

$$\gamma(z) = \sqrt{\frac{z_1^2}{a^2} + \frac{z_2^2}{b^2} + \frac{z_3^2}{c^2}}. \tag{2}$$

This ellipsoid has to be rotated into the orientation of the blood vessel at each point

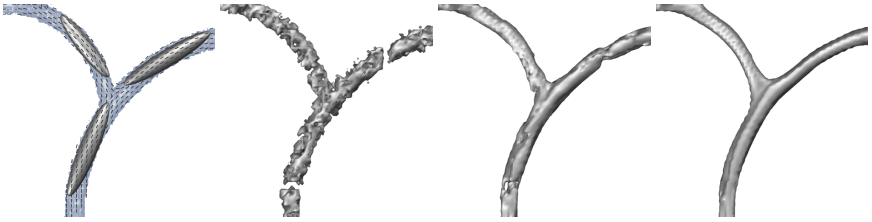

Fig. 3. Left: oriented ellipsoids overlaying a test geometry, right: processing of this geometry with grid size $h \approx 0,015$ and time step $\tau \approx 3 \cdot 10^{-7}$, displayed timesteps 0 (initial data),15 and 70.

(cf. Fig. 3). We consider the local vector $v(x_0)$ for this orientation and restrict ourselves here to a circular cross section in the orthogonal direction and a fixed aspect ratio. In our applications we have considered an aspect ratio ranging from 10 to 100. It is known from Finsler geometry [24] that convex shapes - such as our ellipsoidal shape - appear as minimizers of certain energy functionals. Indeed, given the implicit representation γ (which is supposed to be one homogeneous) we consider a dual function γ^* defined as

$$\gamma^*(z) := \sup_{\|n\|=1} \frac{z \cdot n}{\gamma(n)}.$$

In our case we achieve $\gamma^*(z) = \sqrt{a^2 z_1^2 + b^2 z_2^2 + c^2 z_3^2}$, this is again a function of the ellipsoidal type (2). Now, we take into account this function evaluated on surface normals n as an energy integrant for an anisotropic area functional $E[\mathcal{S}]$ defined on a surface $\mathcal{S}$:

$$E[\mathcal{S}] = \int_{\mathcal{S}} \gamma^*(n)\, da.$$

Up to a scaling the so called Wulff shape $\mathcal{W} = \{z \in \mathbb{R}^3 : \gamma(z) = 1\}$ — in our case the ellipsoid with half-axis a, b, c — locally minimizes this energy [3]. Obviously the structure classification varies with the position on the image domain. Thus, we consider anisotropies $\gamma^* : \Omega \times \mathbb{R}^3 \to \mathbb{R}, \quad (x, z) \mapsto \gamma^*(x, z)$ which in addition depends on this position x. Hence, we have a variational formulation at hand to quantify the coincidence of local structures with the local prior, which is computationally cheap to evaluate and as pointed out in the next section allows for an effective numerical discretization and relaxation.

2.3 Gradient flow

To define the above energy on level sets and level set ensembles, respectively, we integrate the energy over all level sets of a function ϕ, apply the co-area formula, the one homogeneity of γ^*, and obtain

$$E[\phi] = \int_\Omega \gamma^*\left(x, \frac{\nabla\phi(x)}{\|\nabla\phi(x)\|}\right) \|\nabla\phi(x)\|\, dx = \int_\Omega \gamma^*(x, \nabla\phi)\, dx\,. \tag{3}$$

Thus, the first variation of the energy is given by

$$\frac{d}{d\varepsilon}E[\phi+\varepsilon\vartheta]\Big|_{\varepsilon=0} = \int_\Omega \frac{d}{d\varepsilon}\gamma^*\left(x,\nabla\phi+\varepsilon\nabla\vartheta\right)\Big|_{\varepsilon=0} dx = \int_\Omega \gamma_z^*(x,\nabla\phi)\nabla\vartheta\, dx\,.$$

Now, we consider a gradient descent corresponding to this energy and the standard L^2 metric on surfaces:

$$\frac{\partial}{\partial t}\phi = -\mathrm{grad}_{L^2}E[\phi]\,.$$

Following [9] we finally derive the variational formulation

$$\int_\Omega \frac{\partial_t\phi(x)}{\|\nabla\phi(x)\|}\vartheta(x)dx = -\int_\Omega \gamma_z^*(x,\nabla\phi)\nabla\vartheta(x)dx \tag{4}$$

for all test functions $\vartheta \in C_0^\infty$. Our algorithm is now based on a straightforward finite element discretization in space and a semi-implicit backward Euler discretization in time [8]. Due to the minimizing property of the local ellipsoidal Wulff shapes we expect that under this gradient descent the vessel structures will be smoothed and will converge to round tubes. Another advantage of this approach is that small gaps in the vessels will be closed.

Mathematically, this gradient flow is known as the anisotropic mean curvature motion. The isotropic counterpart, classical mean curvature flow (MCF) will nicely smooth surfaces but it is far from being appropriate for long tubular structures like blood vessels (cf. Figure 4). One can introduce the anisotropic curvature h_γ as the first variation of the weighted energy (3) and obtain $h_\gamma(x) = \mathrm{div}\left(\gamma_z^*(\nabla\phi(x))\right)$. Thus, we are lead to the classical formulation of our evolution problem [3]

$$\partial_t\phi = h_\gamma\|\nabla\phi\|.$$

2.4 Local volume preservation

The flow described above uses the anisotropic mean curvature. As this curvature won‘t be zero even for the convex shapes the flow converges to, the objects won‘t stop shrinking until they disappear. As a consequence we need some modification to preserve the volume of objects. The idea is now simply to modify the velocity of the flow in such a way, that the average velocity is zero. This is satisfied if we consider the flow $\partial_t\phi(x) = \left(h_\gamma(x) - h_\gamma^0\right)\|\nabla\phi(x)\|$ with $h_\gamma^0 = \fint_{\phi=0} h_\gamma\, da$. The correction term h_γ^0 is the average anisotropic mean curvature and it is easy to show, that the volume of the object will stay constant under this flow (see for example [22]). However, this global correction is not appropriate for the vessel smoothing problem, because it results in local mass accumulations and deformations. Instead, we use local volume preservation:

$$\partial_t\phi(x) = \left(h_\gamma(x) - h_\gamma^\varepsilon(x)\right)\|\nabla\phi(x)\| \quad \text{with} \quad h_\gamma^\varepsilon(x) = \fint_{B_\varepsilon(x)\cap\{\phi=0\}} h_\gamma\, da.$$

In this flow the local average velocity is only approximately zero, but this is completely sufficient for our method.

Closing gaps in the data. Surfaces that are implicitly given by a level set function, can change their topology in a natural way. This is an advantage for our application since we want gaps in vessels to be closed. If we choose a strong anisotropy term, i. e. we choose the ellipsoid to be very long (e. g. $a = 100, b = c = 1$), then the objects tend to grow into this strong direction. We can accelerate this growth by weighting the volume correction term depending on the normal of the surface and the direction of the vector field v (for normals that are parallel to the direction of the vessel, we want to have no volume preservation) and end up with the flow

$$\partial_t \phi(x) = \left(h_\gamma(x) - \left(1 - \frac{\nabla \phi(x) \cdot v(x)}{\|\nabla \phi(x)\|} \right) h_\gamma^\varepsilon(x) \right) \|\nabla \phi(x)\|. \tag{5}$$

We want to emphasize, that this method will close gaps, even in the total absence of underlying data in the gap (cf. Fig. 4). This is an important difference of our method from previous works. For gaps to be closed, the vector field has to span it. Since we smooth the vector field, this is fulfilled for all small gaps.

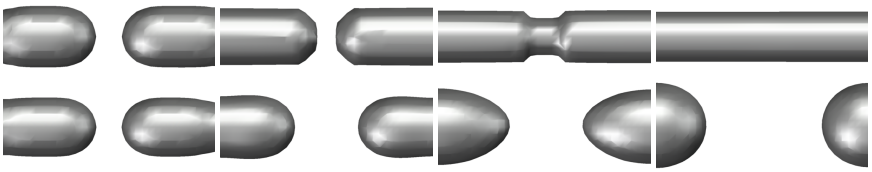

Fig. 4. Top: Gaps in the data set are closed by our approach, even in the total absence of data between the two ends, bottom: Smoothing by the standard morphological method based on volume preserving MCF fails to close the gap.

3 Finite element discretization

Up to now, we have considered a continuous level set function ϕ on the image domain $\Omega \subset \mathbb{R}^3$. Now, we aim at discretizing the approach following the usual finite element paradigms. Due to the highly anisotropic Wulff shapes being considered as local prior the resulting geometric evolution problem not only involves the usual geometric nonlinearities already known from isotropic mean curvature motion but the underlying diffusion will be highly anisotropic. The finite element approach naturally incorporates this anisotropy based on a straightforward discretization of the variational formulation of the evolution problem. In case of a finite difference implementation the reliable treatment would cause serious difficulties. The variational weak formulation of the anisotropic MCF including our volume preservation term is derived as follows. We multiply equation (5) with a test function ϑ, integrate over the domain Ω and apply integration by

parts making use of the above definition of the anisotropic mean curvature. Finally, we obtain

$$\int_\Omega \frac{\partial_t \phi(x)}{\|\nabla\phi(x)\|}\vartheta(x) + \gamma_z^*(x,\nabla\phi)\nabla\vartheta(x)\,dx = \int_\Omega \left(1 - \frac{\nabla\phi(x)}{\|\nabla\phi(x)\|}\cdot v(x)\right) h^\varepsilon_{\gamma^*}(x)\vartheta(x)\,dx$$

where $\vartheta \in C_0^\infty$ is the still continuous test function [3]. Next, we consider the actual discretization in space and time. In the application, images typically arises as arrays of voxels. We interpret voxel values as nodal values on an uniform hexahedral mesh C covering the whole image domain Ω and consider trilinear interpolation on cells $C \in C$ to obtain discrete intensity functions in the accompanying piecewise trilinear and continuous finite element space X^h. For the sake of simplicity, we will assume that $\Omega = (0,1)^3$ and a grid size h. To clarify the notation, we will always denote spatially discrete quantities with upper case letters to distinguish them from the corresponding continuous quantities in lower case letters. With the aim to finally derive a fully practical algorithm we have to incorporate numerical quadrature scheme in case of non polynomial integrant. They are as usual obtained replacing the integrant by a suitable polynomial interpolation. Furthermore, for the discretization in time, we use a semi-implicit backward Euler discretization with τ as selected time step size and use indices to indicate the current time step. Hence we approximate the partial derivative $\partial_t \Phi$ by the difference quotient $\frac{\Phi^{k+1}-\Phi^k}{\tau}$.
Thus, this discretization in space and time lead us to the following discrete problem: Find a sequence of finite element functions $\left(\Phi^k\right)_k$, such that

$$\begin{aligned}
&\int_\Omega I_h^1\left(\frac{\left(\Phi^{k+1}(x) - \Phi^k(x)\right)}{\tau\|\nabla\Phi^k(x)\|_\varepsilon}\Theta(x)\right) + I_h^3\left(\gamma_z^*\left(x,\nabla\Phi^k(x)\right)\nabla\Theta(x)\right)\,dx \\
&= \int_\Omega I_h^1\left(\left(1 - \frac{\nabla\Phi(x)\cdot V}{\|\nabla\Phi(x)\|_\varepsilon}\right)H^\varepsilon_{\gamma^*}(x)\Theta_i(x)\right) - \lambda\frac{\gamma^*(\nabla\Phi(x))}{\|\nabla\Phi(x)\|_\varepsilon^2}\nabla\left(\Phi^{k+1}(x) - \Phi^k(x)\right)\nabla\Theta(x)\,dx
\end{aligned}$$

for all test functions $\Theta \in X^h$. Here I_h^1 denotes the elementwise Lagrange interpolation operator and I_h^3 the interpolation with respect to a Gauss quadrature of third order accuracy. Following the approach of Deckelnick and Dziuk in [8] we have added the second term on the right hand side as a stabilization term. According to their results on numerical analysis, λ has to be chosen such that

$$\lambda \inf_{|p|=1}\gamma^*(p) > (\sqrt{5}-1)^{-1}\max\{\sup_{|p|=1}|\gamma^{*'}(p)|, \sup_{|p|=1}|\gamma^{*''}(p)|\}$$

is fulfilled.
Furthermore (cf. also the fundamental paper by Evans and Spruck [10]) we replace $\|\nabla\Phi^k\|$ by $\|\nabla\Phi^k\|_\varepsilon$, where $\|v\|_\varepsilon := \sqrt{\|v\|^2+\varepsilon^2}$. I. e. we choose $\varepsilon \approx h$. Finally, $H^\varepsilon_{\gamma^*} \in X^h$ is a suitable discrete average mean curvature and $V \in (X^h)^3$ a discrete unit length directional field.

3.1 A fully practical numerical approach

We will now describe in detail, how to define the numerical quadrature rules and the discrete functions $H^{\varepsilon}_{\gamma^*}$ and V. We finally derive the linear system of equations to be solved in each time step. The quadrature rules are given by

$$\int_{\Omega} I^1_h(f) := \sum_C \frac{vol(C)}{8} \sum_{i=1}^{8} f|_C(x_i), \quad \int_{\Omega} I^3_h(f) := \sum_C \frac{vol(C)}{8} \sum_{i=1}^{8} f|_C(y_i),$$

for a function $f : \Omega \to \mathbb{R}$. Here $\{x_i\}$ denotes the set of nodes and $\{y_i\}$ the set of Gauss quadrature points on the hexahedral mesh C. On the unit cube the coordinates of the quadrature points are given by the 8 possible combinations of the weights $\frac{1}{2} \pm \sqrt{\frac{1}{8}}$. In particular for all grid nodes x and for all cells C which share x as a vertex, we consider different gradient evaluations $\nabla\Phi(x)$ on these cells.
We define the discrete directional field V via nodalwise evaluation of the formulas given in section 2. To compute the finite element function H^{ε}_{γ} we first introduce a discrete anisotropic mean curvature function $H_{\gamma^*} \in X^h$ implicitly given by a discrete version of the variational formulation for the anisotropic mean curvature

$$\int_{\Omega} H_{\gamma^*}(x)\Theta(x)\,dx = -\int_{\Omega} \gamma^*_z(x, \nabla\Phi)\nabla\Theta(x)\,dx, \tag{6}$$

for all $\Theta \in X^h$. Let $\overline{\mathbf{H}}_{\gamma^*} = \left(\mathbf{H}_{\gamma^*_i}\right)_{i\in I}$ be the vector of nodal values of the finite element function H_{γ^*}. Here I denotes the index set of the grid nodes. From the above equation we obtain

$$\overline{\mathbf{H}}_{\gamma^*} = -\mathbf{M}^{-1}\mathbf{L}_{\gamma^*}[\overline{\mathbf{\Phi}}^{\mathbf{k}}], \tag{7}$$

where $\mathbf{M}$ is the classical lumped mass matrix defined by

$$\mathbf{M} = \left(\int_{\Omega} I^1_h\left(\Theta_i(x)\Theta_j(x)\right)\,dx\right)_{i,j\in I}$$

(the term on the left hand side of equation (6) is given by $\mathbf{M}\overline{\mathbf{H}}_{\gamma^*}$) and

$$\mathbf{L}_{\gamma^*}[\overline{\mathbf{\Phi}}^{\mathbf{k}}] = \left(\int_{\Omega} I^3_h\left(\gamma^*_z(x, \Phi^k)\nabla\Theta_i(x)\right)\,dx\right)_{i\in I},$$

defines the anisotropic stiffness matrix induced by the anisotropy γ^*. With this function at hand, we can compute a discrete, locally averaged anisotropic mean curvature $H^{\varepsilon}_{\gamma^*}(x_0)$ averaging over all nodal values of the coefficient vector $\overline{\mathbf{H}}_{\gamma^*}$ for nodes within the ε-ball around x_0.
Finally, we formulate the linear system of equations to be solved in each time step. Therefore let $\overline{\mathbf{\Phi}}$ be the vector of nodal values for a finite element function Φ. We then

define a nonlinear mass matrix $\mathbf{M} = \mathbf{M}[\overline{\mathbf{\Phi}}^{\mathbf{k}}]$ and a nonlinear stiff matrix $\mathbf{L} = \mathbf{L}[\overline{\mathbf{\Phi}}^{\mathbf{k}}]$ by

$$\mathbf{M}[\overline{\mathbf{\Phi}}^{\mathbf{k}}] = \left(\int_\Omega I_h^1 \left(\frac{\Theta_i(x)\Theta_j(x)}{\|\nabla \Phi^k(x)\|_\varepsilon} \right) dx \right)_{i,j \in I},$$

$$\mathbf{L}[\overline{\mathbf{\Phi}}^{\mathbf{k}}] = \left(\int_\Omega I_h^1 \left(\frac{\gamma^*(x, \nabla \Phi^k(x)) \nabla \Theta_i(x) \nabla \Theta_j(x)}{\|\nabla \Phi^k(x)\|_\varepsilon^2} \right) dx \right)_{i,j \in I},$$

and complete the system by the right hand side

$$\overline{\mathbf{R}}[\overline{\mathbf{\Phi}}^{\mathbf{k}}] = \left(\int_\Omega I_h^3 \left(\frac{\gamma_z^*(x, \Phi^k) \nabla \Theta_i(x)}{\|\nabla \Phi^k(x)\|_\varepsilon} \right) - I_h^1 \left(\left(1 - \frac{\nabla \Phi(x) \cdot V(x)}{\|\nabla \Phi^k(x)\|_\varepsilon} \right) H_{\gamma_0^*}(x) \Theta_i(x) \right) dx \right)_{i \in I}.$$

Notice, that the anisotropic mean curvature function $H_{\gamma^*}(x)$ has to be recomputed in each timestep. With this evaluation at hand, we finally obtain the following linear system of equations

$$\left(\mathbf{M}[\overline{\mathbf{\Phi}}^{\mathbf{k}}] + \tau\lambda \mathbf{L}[\overline{\mathbf{\Phi}}^{\mathbf{k}}] \right) \left(\overline{\mathbf{\Phi}}^{\mathbf{k+1}} - \overline{\mathbf{\Phi}}^{\mathbf{k}} \right) = -\tau \overline{\mathbf{R}}[\overline{\mathbf{\Phi}}^{\mathbf{k}}],$$

where the initial data Φ^0 is the signed distance function of the thresholded data. In the implementation we solve this linear system of equations with a PCG-solver and a SSOR-preconditioner.
So far we have explained the computation of a single time step. Finally, let us briefly recall the preparatory steps to be performed in advance:

1. Threshold the intensity function I of the MRA data set with an appropriate threshold function α.
2. Estimate the radii of the vessels based upon the resulting discrete characteristic function.
3. Define the narrow band around the vessels using the computed radii.
4. Compute the directions of the vessels based upon the threshold and the radii.
5. Smooth this vector field.
6. Compute the signed distance function of the thresholded image to obtain the initial data Φ_0 for the actual discrete evolution.

4 Numerical Results and Application

We have applied the above anisotropic, locally volume preserving curvature motion approach to real MR angiography data to underline the methods potential for real applications. On the 3D images tubular Wulff shapes are incorporated if the moment analysis and the radii estimate indicate such structures locally. Fig. 3, 4 show the application of our method to test data sets and highlight the capability to close gaps and to ensure nicely rounded cross sections for the tubular structures. By applying level set methods, a d-dimensional problem is transferred into a $d+1$-dimensional space, which results in

more computing time. We reduce the amount of computation by defining a narrow band around the vessels where computation is performed. We only consider grid cells for the narrow band [1] on which the vessel radius estimate returns reliable results (cf. Fig. 11). This leads to a saving of approximately 95% on typical MRA images. After we have estimated the radii and defined the narrow band we perform the remaining preparatory steps only on the nodes in this band.
We have to consider rather small time steps ($\tau \approx 10^{-6} \cdots 10^{-7}$) to avoid too much smoothing due to numerical viscosity. On a 128^3 voxel grid one time step takes about 30 sec on a PC with Pentium IV with 3.4 GHz.
Following the convergence results by Deckelnick and Dziuk [8] the parameter λ has to be chosen as described in section 3. Practically, λ can be chosen much smaller. We have used a constant value $\lambda = 2.5$.
By construction the algorithm will restore and enhance tubular structures. As a first critical test case we take into account branch points on tubular structures. Thus, we consider bifurcations with a different dihedral angle and apply our method to noisy versions of the originally smooth implicit representation of these structures. Fig. 5 demonstrates the robustness of our approach fairly independent of the local branching configuration. As a quantitative measure for the performance we compute the L^1 difference between the original structure (before noise has been added) and our restoration results and compare it with the initial difference for the noisy images.
The next experimental validation concerns highly curved structures and the impact of a varying vessel diameter. Thus, we have applied our algorithm to a 3D image representing an implicit model of a helix with decreasing diameter and increasing curvature of the center line. The result is depicted in Fig. 6, which underlines that even after many timesteps highly curved regions do not deform artificially and the diameter of the structures is sufficiently preserved. Furthermore, we have applied the presented method to actual MRA data sets of the human brain with a resolution $256 \times 256 \times 128$. The data is courtesy of Carlo Schaller, Neurosurgery Hospital at Bonn Medical Center. Fig. 9 and 10 show results of the proposed method on two different data sets.

4.1 Comparison to other algorithms

We have compared our approach to different other methods. Results of this comparison for a 3D MR angiography data set are shown in Fig. 8. To be more explicit, we studied another geometric evolution method designed for the enhancement of co–dimension 2 features on hypersurfaces [19]. As already indicated by Fig. 7 this method is not appropriate for freestanding co–dimension 2 structures and the thin end of the helix disappears. Furthermore, we have also applied isotropic mean curvature motion with a local volume preserving term, characterized by sufficient smoothing but a loss or break up of thinner structures. Clearly, due to the local averaging with a fixed kernel width the local volume preservation can not be ensured on small scales. Finally, we compare our method with the approach by Lorigo *et al.*[18], which also applies to co–dimension 2 vessel structures based on a geometric diffusion in direction of the smallest principle curvature. Here, we applied the implementation by C. F. Westin in the open source package coded in the ITK class *CurvesLevelSetImageFilter*. As shown in Fig. 8

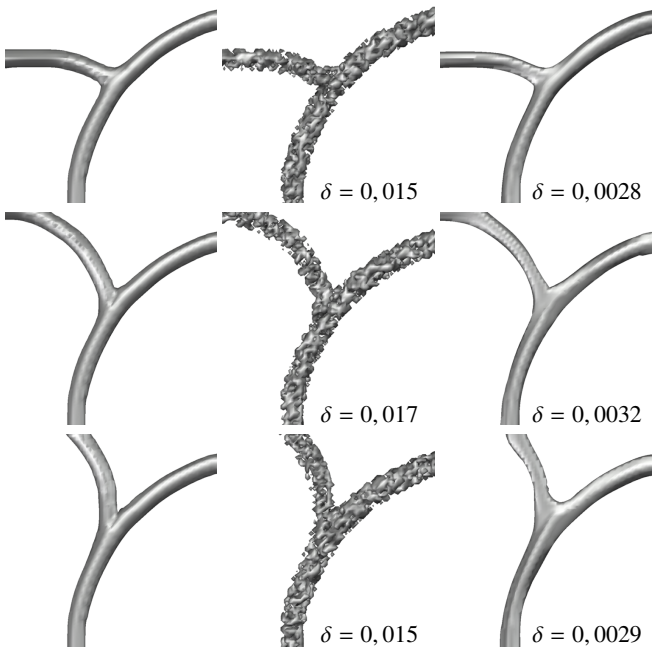

Fig. 5. The algorithm is tested on three synthetic branching configurations with different dihedral angles (first column) which are overlaid with significant noise (second column). The third column shows the restoration results obtained by our method. As a quantitative measure the L^1-norm of the difference of the actual and the original image denoted by δ is plotted for the images in the middle and right column.

some of the thinner vessel structures are better restored either by this or by our method. Overall our approach is characterized by a better denoising. This is due to the fact that our approach combines two diffusion scales: strong diffusion along the in principle co–dimension 2 structures as in the approach by Lorigo *et al.*and in addition on a smaller scale still an evolution towards circular cross sections.

4.2 Limitation of our approach.

The algorithm is well–suited for tubular structures of varying diameter and curvature. Aneurysm and other morbid expansions of vessels are not reflected by the local template construction. Thus, the method will fall back to an isotropic smoothing approach. Furthermore, the method inherently tries to close small gaps along tubular structures. This might be a shortcoming in case of vascular constrictions such as stenosis. Currently, the algorithm is conceived for a feasibility study. So far, apart from the narrow band approach we have not exploited the potential to increase the methods performance with respect to computation time.

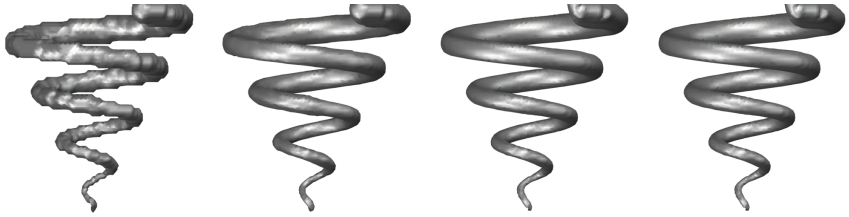

Fig. 6. The algorithm is applied to the implicit representation of a helix with varying diameter and curvature of the centerline. From left to right the time steps 0,100,200 and 500 are depicted demonstrating that the object is smoothed comparably quickly and even over a longer time the geometry of the helix is not effected by the evolution.

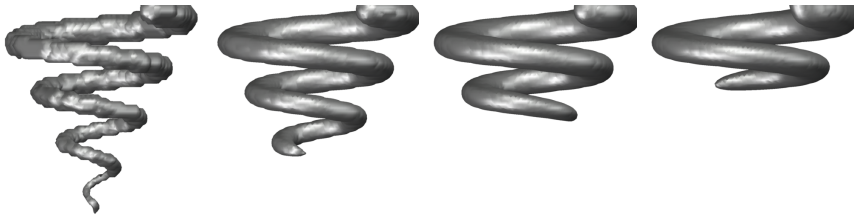

Fig. 7. Application of the geometric anisotropic diffusion approach [19] to the helix test data set.

5 Conclusion and future work

Classical PDE approaches for feature preserving denoising usually fall short in the appropriate processing of thin, elongated structures such as vessels in 3D angiography. Based on a local classification of such tubular structures by elongated ellipsoids as local master pieces and an anisotropic curvature motion model it is possible to preserve and even enhance these structures properly. Thereby, the local anisotropy is explicitly constructed according to the previous classification. As long as gaps in these structures are not too large they can be closed and circular cross-sections are emphasized by the new method. The application to MR angiography is a first case study. Future improvements are required to improve the efficiency of the proposed approach and other application scenarios can be exploited.

Acknowledgment. The authors thank C. Schaller, C. Schlimper, and J. Scorzin from the Neurosurgery Hospital at Bonn Medical Center for providing the MRA data.

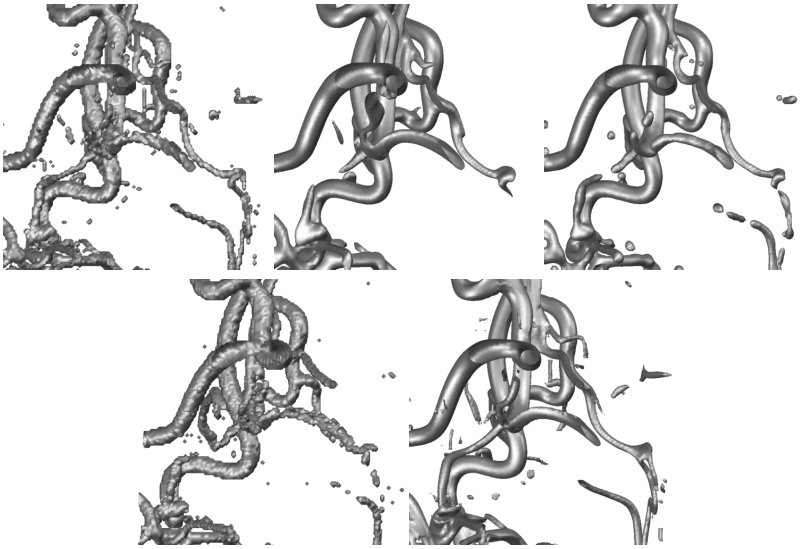

Fig. 8. Comparison of our approach to other methods for a 3D MR angiography data set. The original geometry to be restored is shown in the upper left image. Results obtained by the anisotropic geometric diffusion [19] (upper middle), a local volume preserving isotropic mean curvature motion (upper right), the ITK implementation of the approach proposed by Lorigo *et al.*[18] (lower left), and our method (lower right) are compared.

References

1. D. Adalsteinsson and J. A. Sethian. A fast level set method for propagating interfaces. Journal of Computational Physics, 118(2):269–277, 1995.
2. L. Ambrosio and H.M. Soner. Level set approach to mean curvature flow in arbitrary codimension. J. of Diff. Geom., 43:693–737, 1996.
3. B. Andrews. Volume-preserving anisotropic mean curvature flow. Indiana University Mathematics Journal, 50:783–827, 1991.
4. E. Bullit, A. Aylward, A. Liu, S. Mukherji, J. Stone, C. Coffey, G. Gerig, and S.M. Pizer. 3d graph description of the intracerebral vasculature from segmented mra and test of accuracy by comparison with x-ray angiograms. Information Processing in Medical Imaging (IPMI), pages 308–321, 1999.
5. A. Chung and J. Noble. Statistical 3d vessel segmentation using a rician distribution. Proc. Medical Image Conference and Computer Assisted Interventions (MICCAI), pages 82–89, 1999.
6. U. Clarenz, G. Dziuk, and M. Rumpf. On generalized mean curvature flow in surface processing. In H. Karcher and S. Hildebrandt, editors, Geometric analysis and nonlinear partial differential equations, pages 217–248. Springer, 2003.
7. U. Clarenz, M. Rumpf, and A. Telea. Robust feature detection and local classification for surfaces based on moment analysis. IEEE Transactions on Visualization and Computer Graphics, 10(5):516–524, 2004.
8. K. Deckelnick and G. Dziuk. A fully discrete numerical scheme for weighted mean curvature flow. Numerische Mathematik, 91(3):423–452, 2002.

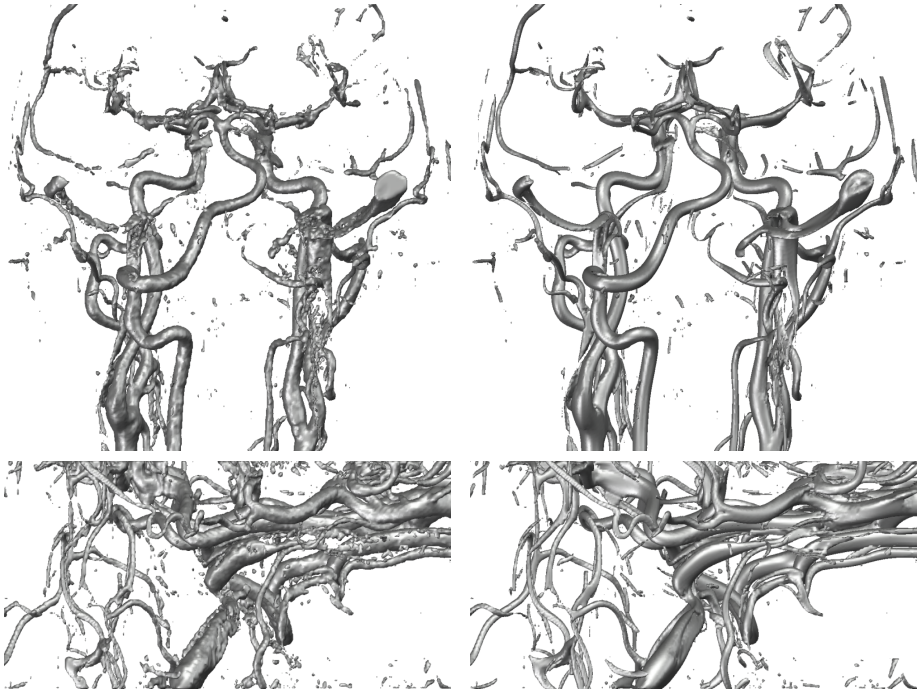

Fig. 9. Application of our method to MRA images (256×256×128 voxels). In the top and second row different perspectives are shown. On the left the original data and on the right the smoothed images after 350 time steps are depicted.

9. M. Droske and M. Rumpf. A level set formulation for willmore flow. Interfaces and Free Boundaries, 6(3):361–378, 2004.
10. L.C. Evans and J. Spruck. Motion of level sets by mean curvature I. J. Diff. Geom., 33(3):635–681, 1991.
11. M.T. Figueiredo and J.M.N. Leitao. A nonsmoothing approach to the estimation of vessel contours in angiograms. IEEE Trans. on Medical Imaging, 14:162 – 172, 1995.
12. A. Frangi, W.J. Niessen, K.L. Vincken, and M.A. Viergever. Vessel enhancement filtering. Proc. Medical Image Conference and Computer Assisted Interventions (MICCAI), pages 130 – 137, 1998.
13. M. Kass, A. Witkin, and D. Terzopoulos. Snakes: Active contour models. International Journal of Computer Vision, 1(4):321–331, 1988.
14. A.K. Klein, F. Lee, and A.A. Amini. Quantitative coronary angiography with deformable spline models. IEEE Trans. on Medical Imaging, 16:468 – 482, 1997.
15. K. Krissian. Flux-based anisotropic diffusion applied to enhancement of 3d angiograms. IEEE Trans. on Medical Imaging, 21:1440 – 1442, 2002.
16. K. Krissian, G. Malandain, and N. Ayache. Directional anisotropic diffusion applied to segmentation of vessels in 3d images. In Proc. Int'l Conf. Scale-Space, pages 345–348, 1997.
17. K. Krissian, G. Malandain, N. Ayache, R. Vaillant, and Y. Trousset. Model based detection of tubular structures in 3d images. Computer Vision and Image Understanding, 80:130 – 171, 2000.

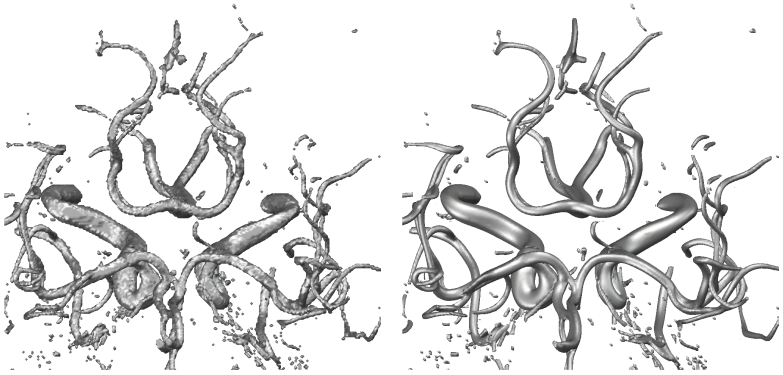

Fig. 10. One more application of our method to a $256 \times 256 \times 150$ MRA image. On the left the original data and on the right the smoothed images after 200 time steps are depicted.

18. L. Lorigo, O. Faugeras, W. Grimson, R. Keriven, R. Kikinis, A. Nabavi, and C. Westin. Codimension-two geodesic active contours for the segmentation of tubular structures. In CVPR'2000, CVPR, pages 444–451, 2000.
19. T. Preußer and M. Rumpf. A level set method for anisotropic geometric diffusion in 3D image processing. SIAM J. Appl. Math., 62(5):1772–1793, 2002.
20. V. Prinet, O. Monga, C. Ge, L. Sheng, and S. Ma. Thin network extraction in 3d images: application to medical angiograms. Int. Conf. on Pattern Recognition, pages 386 – 390, 1996.
21. Y. Sato, S. Nakajima, N. Shiraga, H. Atsumi, S. Yoshida, T. Koller, G. Gerig, and R. Kikinis. 3d multi-scale line filter for segmentation and visualization of curvilinear structures in medical images. IEEE Medical Image Analysis, 2:143 – 168, 1998.
22. J.A. Sethian. Level Set Methods and Fast Marching Methods. Cambridge University Press, 1999.
23. R. Whitaker. Volumetric deformable models: active blobs. Visualization in Biomedical Computing, pages 122–134, Nov. 1994.
24. G. Wulff. Zur Frage der Geschwindigkeit des Wachstums und der Auflösung der Kristallflächen. Zeitschrift der Kristallographie, 34:449–530, 1901.
25. Sun Y., Lucariello RJ, and Chiaramida SA. Directionsal low-pass filtering for improved accuracy and reproducibility of stenosis quantification in coronary arteriograms. IEEE Trans Med Imaging, 14:242?–248, 1995.

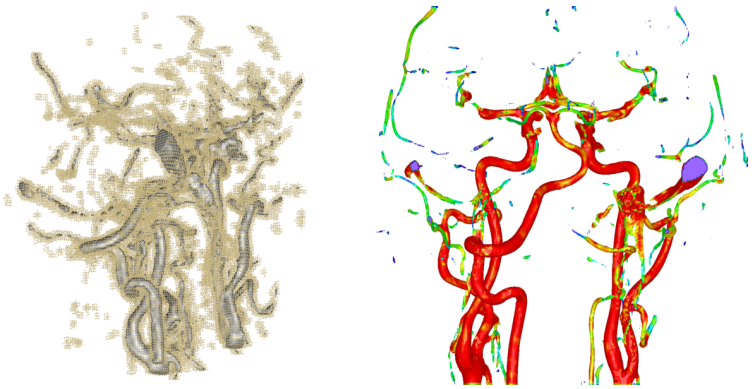

Fig. 11. Left: The vessel structures from image 9 are overlayed with a rendering of the narrow band (yellow dots correspond to nodes in the band), right: The estimated values for the local vessel radius are shown using color coding.